JOURNAL OF THERMOPLASTIC COMPOSITE MATERIALS

Original Manuscript

Design and characterization of electro-active soft actuator based on phase transition of microencapsulated silicon-ethanol composite

Journal of Thermoplastic Composite Materials
2023, Vol. 0(0) 1–20

DOI: 10.1177/08927057231197160
journals.sagepub.com/home/jtc
Sage

Amir Hossein Ebrahimi[1], Hojjat Zamyad[2], Javad Safaei[2] and Samaneh Sahebian[1]

Abstract

In this study, we demonstrate the development of a fast-response soft composite actuator fabricated by mechanical mixing of silicone elastomer (matrix) and ethanol (as phase-change fluid). Joule heating generated by electrical actuation causes a liquid-vapor transition of ethanol embedded in silicone microcapsules; provides the required pressure for mimicking the natural movements. We discuss the critical design variables to improve the temperature response, chemical composition, mechanical properties, force generated, and microstructure of soft actuator. Our soft actuator produces a high load-to-weight ratio (1000 times greater than its own) using a low-voltage source (˜20V). The stability of the soft actuator under multiple working cycles would bring the application to different robotic areas. The actuator using the mechanism presented here is easy to manufacture, automate, and recyclable. It can be used in a range of robotic applications.

Keywords

Soft actuator, silicone, ethanol, phase change material, thermal analysis, microstructure, micro-encapsulation

[1]Metallurgical and Materials Engineering Department, Faculty of Engineering, Ferdowsi University of Mashhad, Mashhad, Iran
[2]Department of Electrical Engineering, Faculty of Engineering, Ferdowsi University of Mashhad, Mashhad, Iran

Corresponding author:
Samaneh Sahebian, Department of Metallurgical Engineering and Materials Science, Faculty of Engineering, Ferdowsi University of Mashhad, Mashhad 9177948974, Iran.
Email: s.sahebian@um.ac.ir

Introduction

Biology has been a source of inspiration for researchers to mimic natural design functionality and develop soft-bodied programmable motion. By combining body compliance and mechanical properties, soft robots have made it possible to develop complex human-or animal-like functions such as walking, crawling, climbing, and gripping.[1–7] Owing to lightweight, excellent capability of adapting to complex environments, and coexisting interaction with humans, soft robots are robust alternatives to convectional robots.[8–10] They have found various applications in drug delivery, biomedical systems, robotic manipulators, etc.[11–14] While rigid-bodied robotics is a successful field, they incur inherent disadvantages that can bring limitations in other circumstances: such as non-collaborative, high cost and weight, and thermodynamic non-efficiency.[1,15–17] There has been growing interest in overcoming such constraints by developing soft actuators in recent years. Soft robots compete with their rigid counterparts in the robotics research community.

One of the long-standing challenges in soft robotics stems from the lack of materials combining actuation, self-awareness, and computerized control.[15] Several types of soft actuators have been explored to design high-performance soft robots, such as shape memory polymers (SMP), shape memory alloys, hydraulic or pneumatic fluidic elastomer actuators, electrorheological materials, and ionic polymer-metal composites (IPMC).[18–28] Robinson et al.[29] demonstrated pneumatic artificial muscles arranged in a parallel bundle with independently controlled motor units that can emulate the structure and operation of human skeletal muscle. Jin et al.[30] prepared a single-component soft robot using a programmable crystalline shape memory polymer with thermo- and photo-reversible bonds, which can be programmed into various soft robots, including a 3D crane and an elephant. Each technique mentioned above can be prohibitively consuming energy and require additional equipment. For example, high voltages are needed to trigger electroactive polymers (>1KV), and pressure-regulating components (pumps, valves, and compressors) for hydraulic or pneumatic fluidic elastomer actuators are required, which limit their miniaturization and applications.

Many forms of soft actuators have emerged in recent years due to the advent of new materials and new fabrication methods.[31–36] Phase change materials (PCMs) are a group of substances that utilize phase change to transform thermal energy into mechanical work based on a rapid expansion at phase transition temperature.[37–41] Recently, liquid-vapor PCM offered an attractive alternative to conventional electromechanical actuators. Zhou et al.[42] fabricated an electrothermal phase transition actuator based on a super aligned carbon nanotube film and elastomers consisting of injected water into an enclosed cavity. The actuated membrane can lift a 500*g* object as a result of heating 2.5 mL encapsulated water under applied voltage (<100V). Chellattoan et al.[43] demonstrated low voltage-driven soft actuators based on phase transition. They reported large motion in <7 s by the electrically induced phase transition of a fluid in a cavity. Miriyev et al.[44] have developed ethanol-gas phase transition composites that exhibited a high strain (up to 900%) and correspondingly high stress (up to 1.3 MPa) with low density (0.84 gr/cm^3). However, the material-actuator exhibited failure after three additional cycles due to the rapid escape of

ethanol from the material. Also, after a few cycles, the temperatures reached the values at which silicone elastomer rapidly degrades.[45]

In this study, we develop a novel programmable electro-responsive soft actuator based on a liquid-vapor transition of microencapsulated ethanol located throughout the silicone matrix. The actuator is a low-voltage-driven (less than 20 V), compact and multifunctional system. To realize the aim, we performed a comprehensive characterization on the material working mechanism and the relationships among composition, structure, and properties; in response to roboticists' demands to design soft actuators that meet their bespoke needs. The characterization data for this study was obtained through thermal and compositional analysis, exploration of material microstructure using electron microscopy, and assessment of material mechanical properties. As a part of this investigation, we also assessed the locomotion power value and the internal temperature effects on the force generated by the material. We optimized silicone-ethanol ratio by characterizing the actuator with different ethanol content, and multi-cyclic actuation tests were performed to evaluate the durability of the actuator. The proposed soft actuator demonstrates a high load-to-weight ratio (1000 times greater than its own) and repeatable expansion. Furthermore, as shown later, the soft actuator is used in various robotic applications, such as artificial grippers. To the best of our knowledge, no research that focuses on identifying the key parameters guiding the performance of such a thermofluidic system has been done to design an electrically driven, compact, and better performing phase change actuator.

Materials and methods

Materials

In this study, a two-component room temperature vulcanized (RTV) silicone elastomer was used as the matrix, which is environmentally friendly, safe, and has excellent processability (Haotian, China). Ethanol (>99.5%) was used as PCM, with physical, chemical, and economic requirements, namely suitable phase change temperature, non-toxicity, and low price. Ethanol was purchased from Merck (Germany). A 0.25mm-diameter nickel-chromium resistance wire was used for electrically-driven actuation of the composite by Joule heating.

Preparation of liquid-silicone elastomer composite

The functional composite was synthesized by mechanical mixing of 5, 10, and 15 wt% of ethanol with the silicone elastomer. The findings indicated that the preparation of the composite with 20 wt% of ethanol and more, in addition to the difficulty in the mixing process, led to phase separation in the chamber. After mixing the silicone with ethanol for 5 min, a hardener with a weight ratio of 1 to 50 was added to the mixture. Note that the media were weighted regularly during the process to retrieve ethanol volatilized. In this research, the molding process was performed in a polymethyl methacrylate (PMMA) mold (15 × 15 × 90 mm dimensions) with a pre-installed thermistor and Ni-Cr wire in a spiral shape inside it. Ni-Cr resistance wire with a length of 75 cm was wound into a spiral

by twisting around a shaft. After molding, the actuator was cured for 4 h. Figure 1 shows a schematic of the PCM-elastomer composite fabrications method, the shape of the mold, and the as-cured sample.

Characterization

The nanocomposite microstructure was evaluated by field emission scanning electron microscopy (FESEM, MIRA3 TESCAN, Czech Republic) at an accelerating voltage of 10 kV. Samples were cryogenically fractured in liquid nitrogen and coated with a thin layer of platinum before the observation. Olympus BX41M-LED (Japan) optical microscope was used for optical characterization of the actuators. Tensile tests were carried

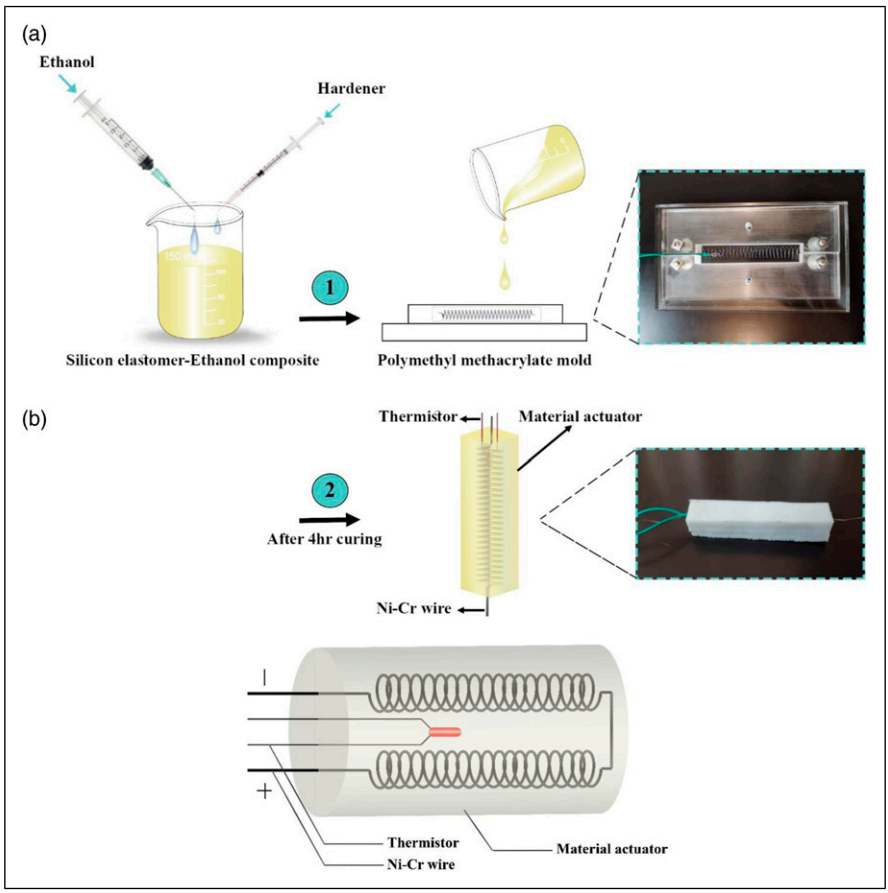

Figure 1. (a) Schematic of the composite preparation method, the shape of the mold, along with the cured actuator, (b) Cylindrical actuator prepared for blocked-force characteristics.

out at room temperature (20°C) using a universal testing machine (UTM, Zwick 250, Germany) at 500 mm/min crosshead speed. The specimens were prepared according to ASTM D-412, type A. The force generated by the actuator was measured using a 500N load sensor. The cylindrical actuator samples (50 mm long, 2.5 mm diameter) were prepared for the blocked force experiment. First, a suitable casing was designed to constrain the motion of the actuator in all directions except at the actuator tip. Another flat rectangular surface was prepared and attached to the load sensor. Once the actuator was electrically actuated, the tip was allowed to apply force on the sensor through the flat surface; the force generated was then monitored using a computer. Thermogravimetric analysis (TGA) was applied at 25°C–300°C temperature range and a heating rate of 10°C/min. Sample decomposition was studied in the air environment, and measurements were performed using the TGA instrument (Shimadzu, Japan). The Joule heating generated by resistive wire was measured using pt1000 and lm35 sensor (Japan), capable of measuring up to 300°C. The NEC Avio Infrared compact thermal camera (Japan) measured the thermal response of actuator and heater design. The actuation performance was evaluated for different input energies (10, 15, 20, and 25 W) by capturing the deformed shape using a video camera (Canon, Japan). The image processing was conducted by MATLAB software, similar to Zamyad et al.[46] Composite performance was evaluated under four different powers (10, 15, 20, 25 W) in the first, second, and third periods corresponding to days 1, 3, and 6. Samples are named SEx which means silicone-ethanol composite and x is a number showing the actuation power in watts.

Result and discussion

Selection of the optimal value of ethanol

As shown in Figure 2(a), the internal pressure inside the soft body actuator is almost zero before electrical actuation. Composite performance becomes faster as heating continues beyond the boiling point of ethanol (T= 78.32°C). The electrical actuation of the actuators by Joule heating provides a vast volume expansion due to the vapor pressure induced by the liquid-vapor transition in the microcapsules. The micropores distributed throughout the polymer matrix are visible in the optical image of Figure 2(a).

Thermal stability is a key factor in the thermo-active cyclic performance of PCM, which determines the availability and working durability of phase change materials.[47–49] For this reason, the thermal stabilities of the silicone-ethanol composites in different weight ratios (0, 5, 10, 15 wt%) were detected by TGA (Figure 2(b)). For SE15, a drastic weight loss takes place between 45 and 100°C because of the evaporation of ethanol out of the microcapsules. At around 120°C, ethanol completely evaporated from the microcapsules (overall, about a 15% decrease in weight was noted). The weight loss value corresponding to 45°C for SE15 is about 4.8%, while 1.8% and 1.2% for SE10 and SE5, respectively. The latter may be attributed to the smaller weight ratio of ethanol/silicone, which encapsulated less ethanol by a greater amount of silicone. The TGA spectrum pertaining to the 10 wt%-ethanol composite showed similar behavior where the total weight loss was measured at about 10%. The TGA curve of 5 wt%-ethanol composite

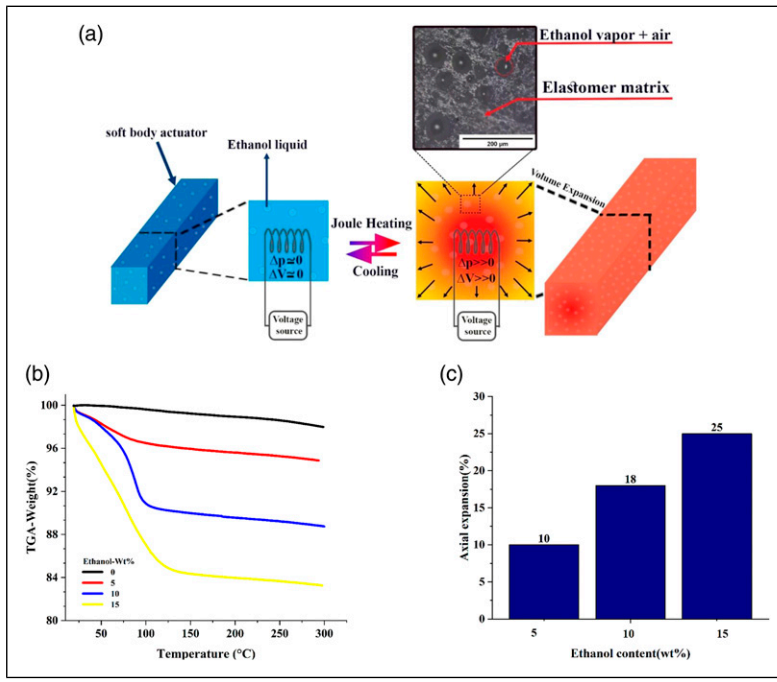

Figure 2. (a) Working principles of stimuli-responsive soft actuator, (b) Thermogravimetric analysis (TGA) spectra for the ethanol/silicone composite containing 0–15 wt% ethanol and c-Displacement and a corresponding axial expansion under similar actuation condition for 5 wt%, 10 wt%, and 15 wt% ethanol.

exhibited a minor change around 45°C. This may be attributed to the relatively low initial ethanol amount. No significant weight loss occurred after 125°C in all composite samples. In contrast, the TGA curve of the pure silicone elastomer had no changes in the 50°C–100°C temperature range, and the total weight loss was measured for this specimen via TGA analysis of about 1.98%. As shown in Figure 2(b), it is notable that the residual ethanol in silicone microcapsules is significantly affected by the weight ratio of ethanol/silicone. When the samples were synthesized with the higher weight ratio of ethanol to silicone, the microcapsules obtained had lower residual ethanol than others.

In most animals, muscle contraction is restricted by the joints, which causes less than 20% fiber tension.[50] Therefore, achieving an expansion strain value equivalent to at least 20% of the initial length was considered to select the optimal value of transformable liquid to meet the purpose of the study. Accordingly, three composite samples comprised of 5, 10, and 15 wt% ethanol were prepared by embedding 75cm of nickel-chromium wire. All samples were triggered under similar electrical actuation conditions (0.5A×20V=10 W). Figure 2(c) shows the heat-triggered elongation as a function of ethanol content in composites. As can be seen, there is ascending proportion of axial expansion by increasing ethanol content, while the heat-triggered elongation of 15 wt% ethanol sample

achieved the least 20% of the initial length. Therefore, 15 wt% was selected as the optimal measured value of phase change fluid in the composite.

Thermal properties assessment

Figure 3 shows the temperature response of composite samples in three actuation periods as a function of driving power. As shown in Figure 3(a), there is a noticeable decrease in total working time by increasing applied power from 10 to 25 W. While it takes about 9300 s to complete 10 working cycles for the SE10, the latter decreases to 3600, 2600, and 2100 s for the SE15, SE20, and SE25, respectively. This can be attributed to the value of input heat flux, which plays a critical role in the thermo-responsive performance of soft actuator and affects the liquid-vapor phase transition rate.

As seen in Figure 3(a), there is a descending trend in the frequency of average maximum value of surface temperature in the first actuation period in which by increasing of applied power from 10 to 25 W, the latter decreased from 45.6 to 34°C. The slow rate of input heat flux at low powers (10 and 15 W) provides more time to transfer thermal energy from internal layers of the actuator to the surface. The latter may result in homogeneous heat distribution throughout the sample. The findings reveal that the actuators show a stable temperature response in which the highest recorded internal temperature was ~73°C after applying 10 working cycles.

The samples were tested on the third day (second actuation period) under electrical actuation conditions similar to the first day. As can be seen in Figure 3(b), the total working time of all samples increased on the third day, which can be attributed to the depletion of ethanol during the first prolonged actuation and formation of passive-elastic outer layers around them. As the capsuled liquid in each lateral micron-scale pocket is evaporated, it leaves an ethanol-free residual layer that acts as one- a barrier to reach the heat-triggered length, which extends the total working time, and two- a protective layer against more depletion of ethanol located in inner microcapsules. As shown in Figure 3(b), longer actuation time caused receiving more input heat flux by samples, which increased the internal temperature of all samples compared to the first day. The average maximum value of internal temperature for all samples increased in the second actuation period, and the latter is the most for SE25, which changed from 68.8 to 86°C (up to 20% growth).

The ethanol content is the lowest in the third actuation period (sixth day). The escape of ethanol in the first and second actuation periods provides extreme conditions, resulting in a significant increase in total working time and internal temperature of composite actuators (Figure 3(c)).

Chemical composition analysis

The effect of multi-cyclic electrical actuation on the chemical composition of composite samples was investigated by weighing the samples before and after each working period. Figure 4(a) shows the residual ethanol in composite samples at the end of the first and second electrical actuation periods. As shown in Figure 4(a), more than 20 wt% of the

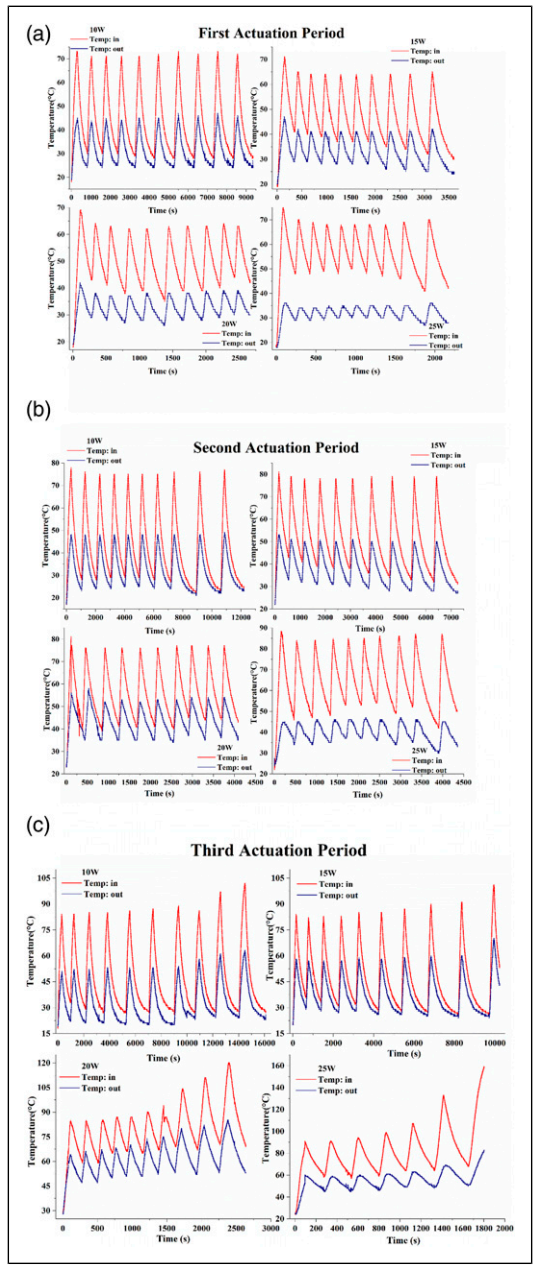

Figure 3. Temperature response characteristics of electrically-driven actuation of the composite by Joule heating at cyclic actuation (15 wt% ethanol). Internal and surface temperature plotted against time at (a) first actuation period (Day 1), (b) second actuation period (Day 3), (c) third actuation period (Day 6).

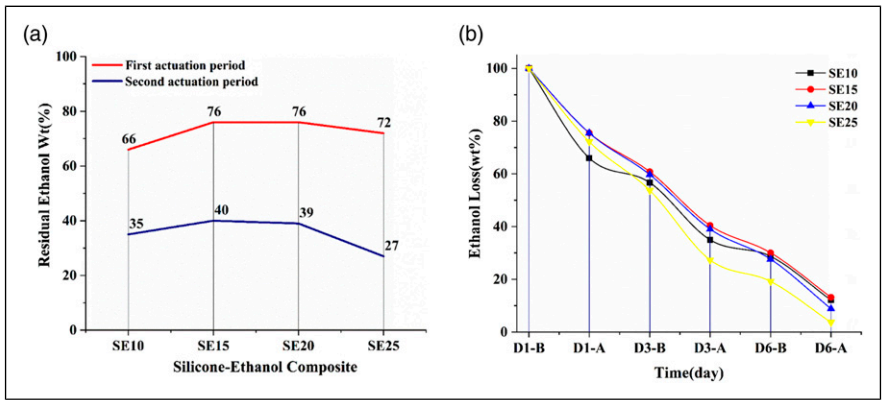

Figure 4. Analysis of chemical composition of soft actuator using ethanol at different power inputs. (a) residual ethanol content at the end of first and second actuation period, (b)-Total ethanol loss during actuation periods.

active phase was released from the composites at the end of the first period. Compared to other samples, the residual ethanol is lowest in SE10 due to the slow input heat flux rate and longer total working time. The same level of ethanol evaporation in SE15 and SE20 may be explained by receiving equal thermal energy (actuation time * power ~ 12.8Kj). As can be seen in Figure 4(a), there is a marked decrease (over 30%) in residual ethanol in the second actuation period, which can be attributed to extended total working. As can be seen, the proportion of ethanol escape is similar to the first actuation period, while SE25 possesses the lowest ethanol index. This may be explained by the higher internal temperature, around 10°C more than other samples.

Findings reveal that the actuator's residual ethanol is significantly affected by the value of driving power. The microcapsules actuated at power 10 and 25 had lower residual ethanol than the others, which can be attributed to the slow rate of input heat flux and thermal shock at low and high power, respectively.

Mechanical properties

Figure 5(a) shows the typical stress-strain curves of pure silicone and silicone-ethanol composite at room temperature. The samples exhibited rubbery behaviors without yield, necking, or strain hardening. It may be seen that the optimal measured value of ethanol (15 wt%) affects the mechanical properties of the composite. Findings reveal a significant decrease in elastic modulus (1.11 to 0.2 MPa, Figure 5(b)) and tensile strength (3.72 to 1.05, over 70% reduction), while the elongation at break increased up to 200%. The incorporation of ethanol reduces the entanglement of the silicone chains. It provides more free volume, which causes the polymer chains to stretch easily at a specific level of tension. Also, the weaker mechanical properties of the silicone-ethanol composite can be attributed to a decrease in the mass of the solid phase (silicone) replaced by ethanol with no reinforcing effect.

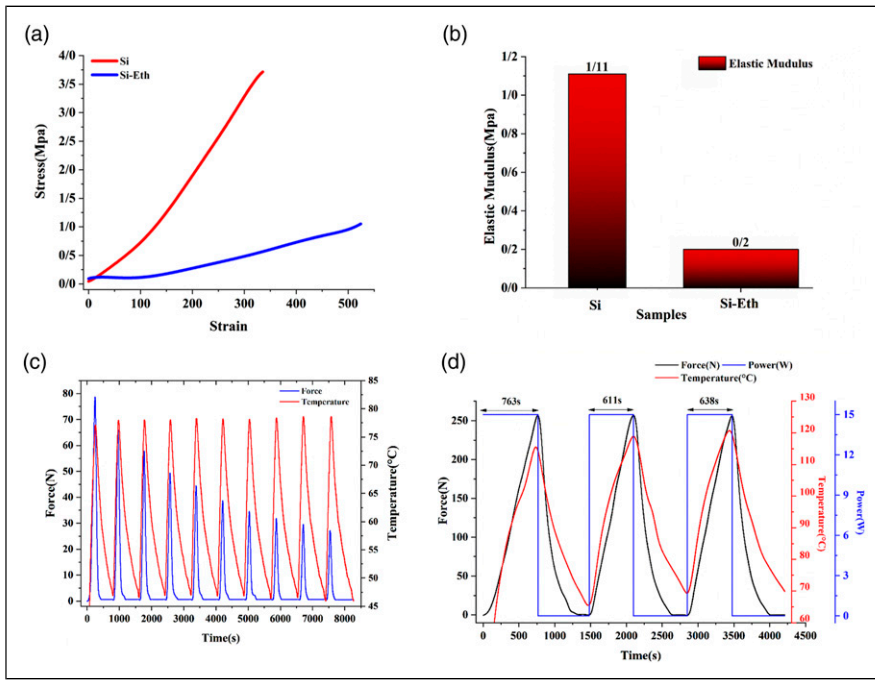

Figure 5. Mechanical properties of pure silicone and as-cured silicone-ethanol composite, (a) stress-strain behavior, (b) elastic modulus, (c) multi-cyclic blocked-force analysis for 15 W power input, d-maximal force-temperature correlation for the 15 wt% composite.

Figure 5(c) illustrates information regarding the blocked-force characteristics of soft actuators prepared in a cylindrical shape (Figure 1(b)). In each cycle, the composite actuator was triggered via Joule heating to exert a temperature of 78°C (boiling point of ethanol) and then de-actuated by ambient cooling until the exerted temperature decreased to 45°C. A further decrease in room temperature was avoided, which is significantly time-consuming. As can be seen in Figure 5(c), in the first cycle, the achievable force corresponding to T=78°C reached a peak of ~80*N*, then faced a gradual decrease for the subsequent nine cycles, and finally dropped to ~30 N in the tenth cycle. This may be attributed to ethanol's loss, which resulted in weaker actuator functionality. It is notable that the actuator succeeded to produce heat-triggered force 100 times greater than its own (25 gr) in the last cycle.

Figure 5(d) shows the force generated by the soft actuator equal to 1000 times of its own weight (~25 gr) to characterize force-temperature correlation. Under 15 W, the pristine actuator could generate a ~250 N force in 763 s, but with the preheated system, it took 611 s to generate the same force. In the first cycle, the internal temperature stood at the lowest point (115°C), which was 5°C less than the third cycle. The required time for

achieving the maximum force value increased from 611 to 638s in the third cycle, which may be explained by the evaporation of ethanol from capsule structure of actuator.

Strain characteristic

The thermo-responsive behavior of the soft actuator is shown in Figure 6-a-b. We used a thermal camera to characterize the ability of the Ni-Cr wire to heat the surrounding actuator composite and heat distribution throughout the sample. As shown in thermal and digital images of Figure 6(a), the current is forced to flow directly from one end to the other through the spiral path by implementing the Ni-Cr wire heater in the composite, which brings heat through the majority of the composite, allowing for even actuation. The temperatures in the tips of the actuator (~55°C) are less than the middle (~80°C), due to the more sidewalls in touch with environment and connecting to clamp.

As shown, the performance of actuator is slow at the beginning of the actuation (45°C, 150 s), but as the actuation continues and the internal temperature rises from 45 to 75°C, the vapor pressure inside the microcapsules increases. This is followed by a better electrically actuation response and rapid movement. The actuator shape recovery process occurs dramatically within the initial seconds of relaxation time due to the fast strain energy dissipation of the specimen. This can be seen in relaxation images of Figure 6(a) when the shape recovery becomes approximately complete over a 150 s period (between 300 and 450 s).

For further evaluation, we measured the velocity of the tip of the actuator at similar locomotion power (10 W) in two different states: one- pristine actuator (first cycle, $T_{initial}$=20°C) and two- preheated actuator (second cycle, $T_{initial}$=45°C). Figure 6(a) presents information regarding to velocity of the actuator and the effect of preheating on this value. As shown, in the first 150 s, the pristine actuator shows negligible forward motion, and the velocity is stabilized at 0.018 mm/s due to the gradual boiling of ethanol. Then, followed by a steady temperature increase to 78.3°C, the soft actuator reaches the maximum heat-triggered elongation (25% of initial length) when it moves at = 0.066 mm/s. In the reverse direction (relaxation time), the velocity of the actuator dramatically changed from 0 to 0.3 mm/s during the first 15 s, which can be attributed to the fast elastic energy dissipation. A similar trend is observed over time when the variation of the shape recovery becomes inconspicuous. The further decline in velocity from 0.3 to less than 0.05 mm/s is due to the termination of strain energy. At the end of the relaxation time, the internal temperature of the sample is approximately 45°C (Figure 6(b)). In the second actuation cycle, the pre-heated system needs less actuation time (215 s, Figure 6(b)), and the slope of velocity graph increases sharply in the forward direction due to the part of the supplied energy was stored in the system as internal energy (Figure 6(c)). After this, the value of the maximum velocity of the actuator in forward direction increased 40%. The slight decrease in maximum value of velocity in reverse direction (from 0.3 to 0.28 mm/s, 6%) can be attributed to the more induced vapor pressure in the preheated system that acts as a barrier to reaching the initial length.

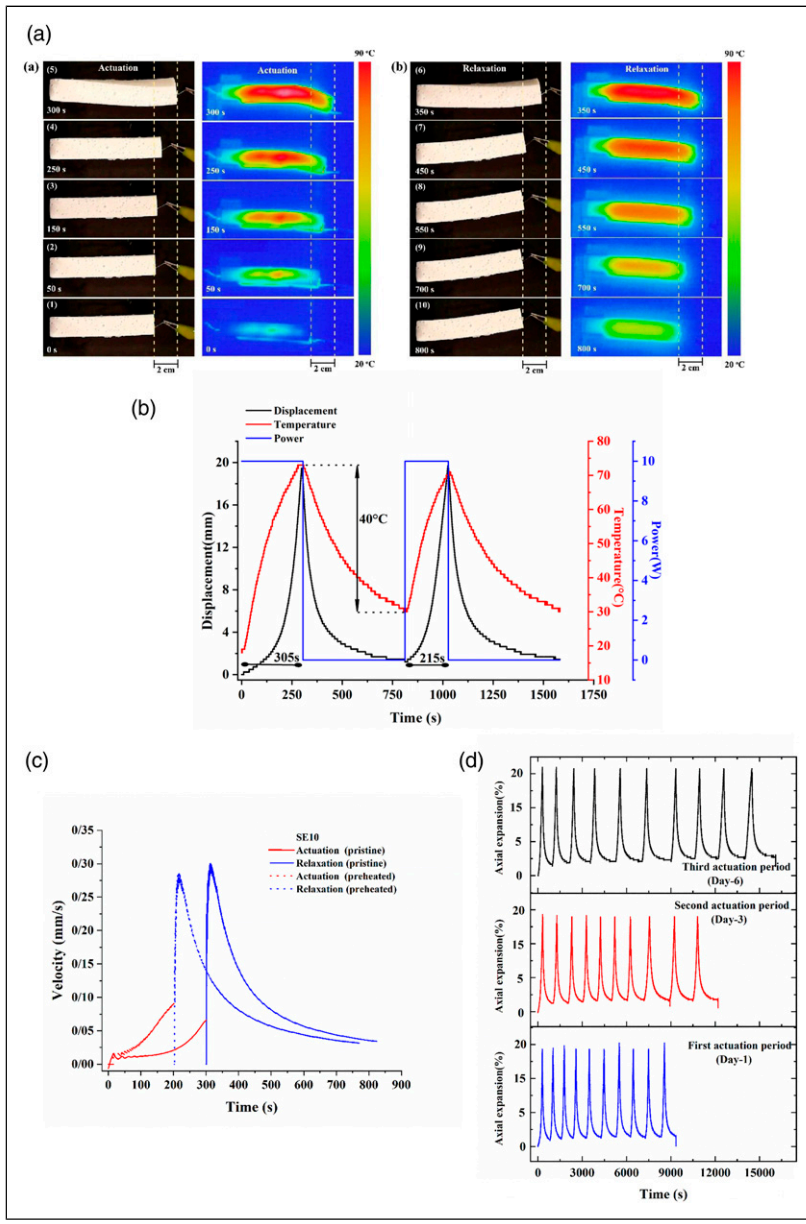

Figure 6. (a) thermal-digital images of a pristine sample Joule heated with 10W of power, (b) displacement-temperature-power correlation for 10 W power input, (c) velocity of the tip of the actuator at similar locomotion power (10 W) in two different states, pristine and preheated, (d) Strain characteristics of silicone-ethanol composite actuator (15 wt% ethanol) at 10 W locomotion power.

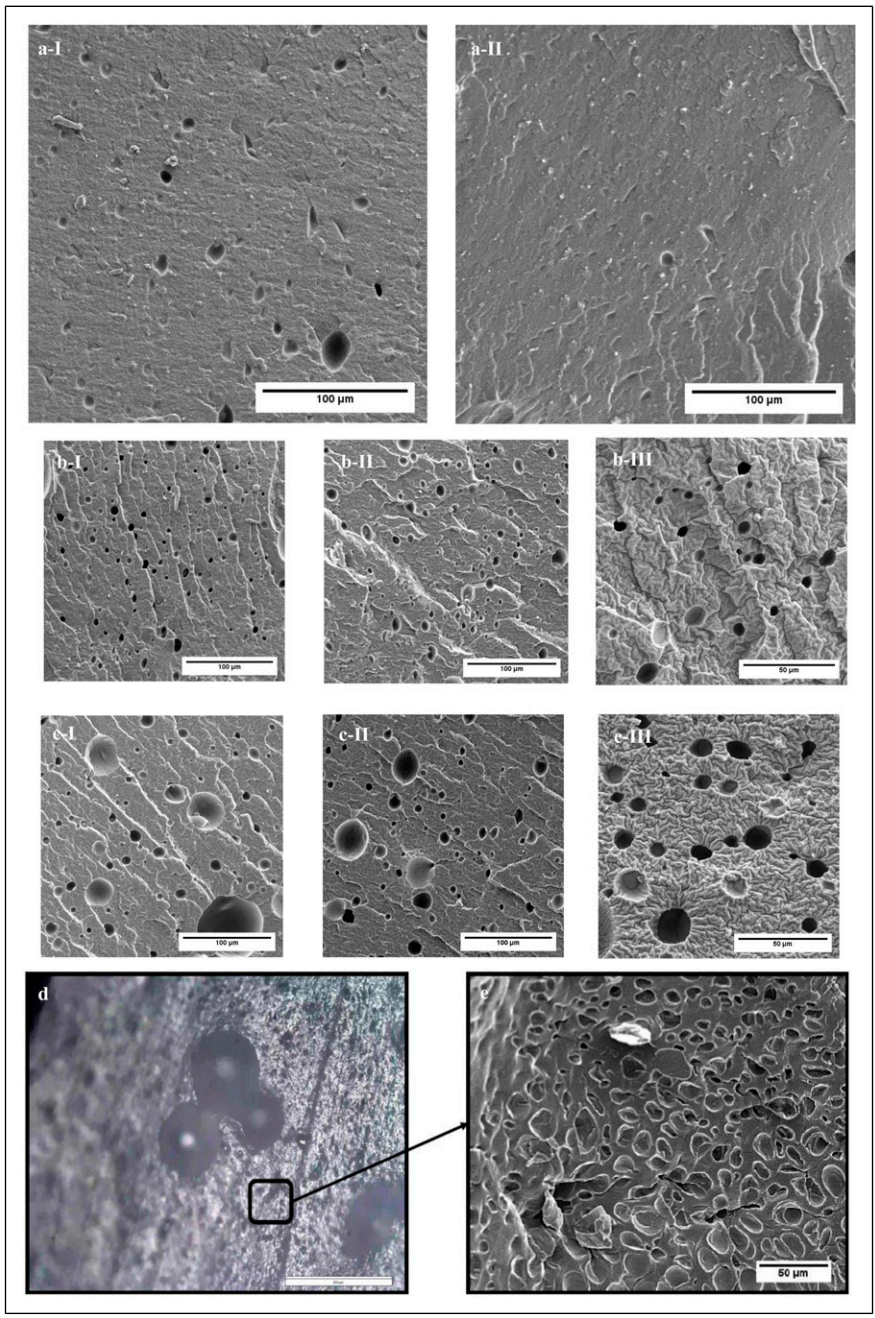

Figure 7. FE-SEM images of SE10 and SE25 composite microstructure. Outer layers: (a I) (SE10) and (a II) (SE25); Internal layers: (b I–III) (SE10), (c I–III) (SE25), (d) optical and (e) FE-SEM images of adjacent microcapsules of SE10.

Figure 6(d) shows strain characteristics of soft actuator (15 wt% ethanol) at cyclic actuation (locomotion powered at 10 W). A visual comparison between strain-time curvatures reveals the limitation of repeatable expansion in different actuation periods. The multiple working cycles increase the actuation durability by two key factors,

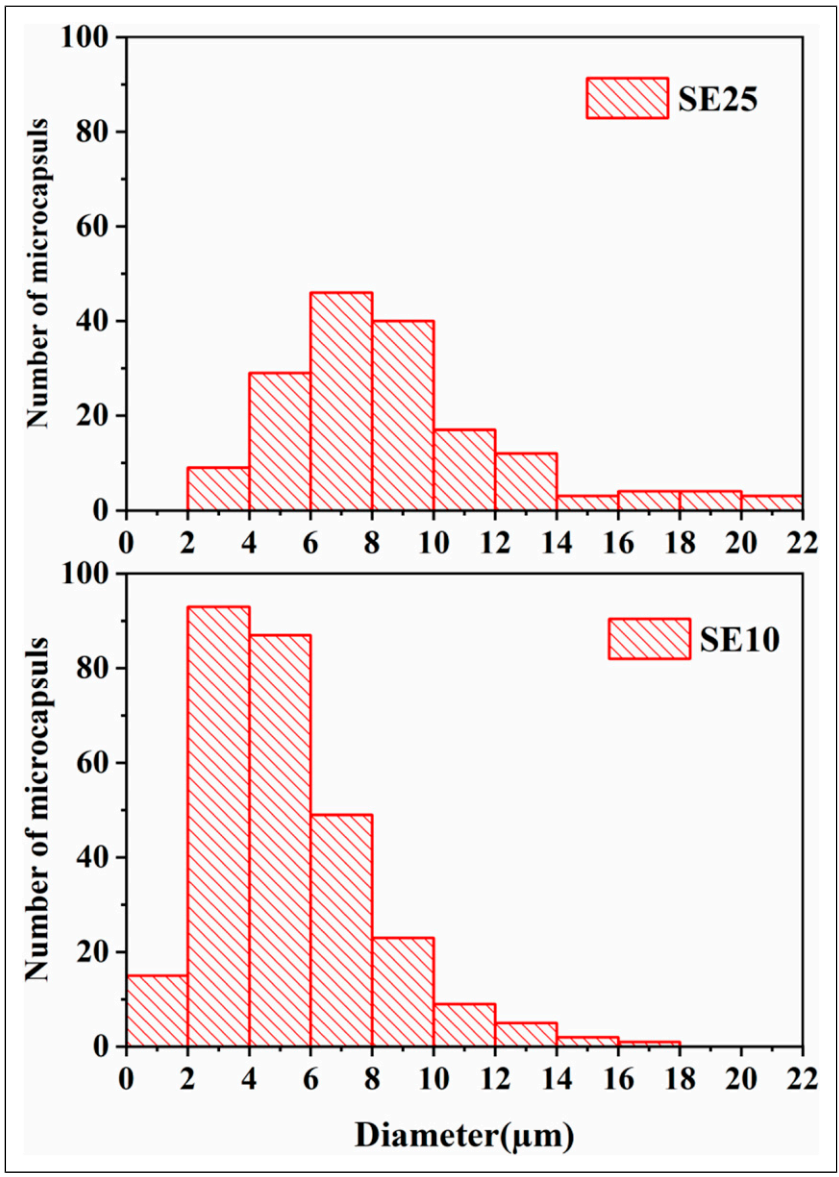

Figure 8. Frequency distribution of microcapsules diameter in internal layers of SE10 and SE25.

1-ethanol escape, which resulted in a reduction of excitability of the actuator and limitation of extending the life cycles, 2-formation of passive outer layers acts as a barrier against soft actuator heat-triggered elongation.

Material microstructure

To investigate the effect of long-term electrical actuation and applied power value on silicone-ethanol composite microstructure, SE10 and SE25 samples were cryogenically fractured after 10 working cycles in the third period. The fracture surface was observed by field emission electron microscopy (Figure 7). It is obvious that hand-mixing of 15 wt% ethanol with silicone elastomer matrix has resulted in a homogeneous distribution of active phase across the entire composite volume. The separation of micron-scale pockets allows the distribution of encapsulated liquid in small quantities across the entire matrix volume. As shown in Figure 7(a-I-II), the number of ethanol encased in the micro-pockets near the outer layers of SE10 is more than SE25, which can be attributed to the higher surface temperature in SE10 (~60°C) and heat concentration in the core of SE25.

As seen in Figure 7(b-c), the microcapsules located in the core of SE10 are smaller and distributed more uniformly than SE25. To verify these observations, the diameter-size distribution of microcapsules located in the inner layers of composite samples was evaluated, and the results are presented in Figure 8 and summarized in Table 1. According to Figure 8, the number of microcapsules in an equal scanned surface area in SE10 is more than SE25. Also, the main diameter size distribution of microcapsules varies in the range of $2< D\ (\mu m)< 8$ and $4< D\ (\mu m)< 10$ for SE10 and SE25, respectively. The data presented in Table 1 reveals a much more significant surface area (more than twice) and higher average diameter (more than 25%) in SE25 than in SE10. High ethanol depletion and thermal shock in SE25 limited its actuation functionality; therefore, higher vapor pressure was needed to achieve determined elongation, which causes a large plastic deformation within the matrix and merging the small microcapsules. The optical and FE-SEM images of Figure 7(d-e) shows large interconnected cavities (60μm) next to small capsules (3μm) in SE25.

Implementation in robotics

In Figure 9, We demonstrate the versatility of our electrically driven actuator as a soft gripper. As shown in Figure 9(a), we designed a biomimetic robot comprised of a silicone-ethanol composite attached to a passive layer (un-actuated) of pure silicone elastomer. During the actuation, the sample expands radially due to the incommensurate asymmetric

Table 1. Microcapsules characteristics.

Samples	Average value of diameter (μm)	Average value of surface area (μm)
SE10	4.6	16.1
SE25	6.3	32.6

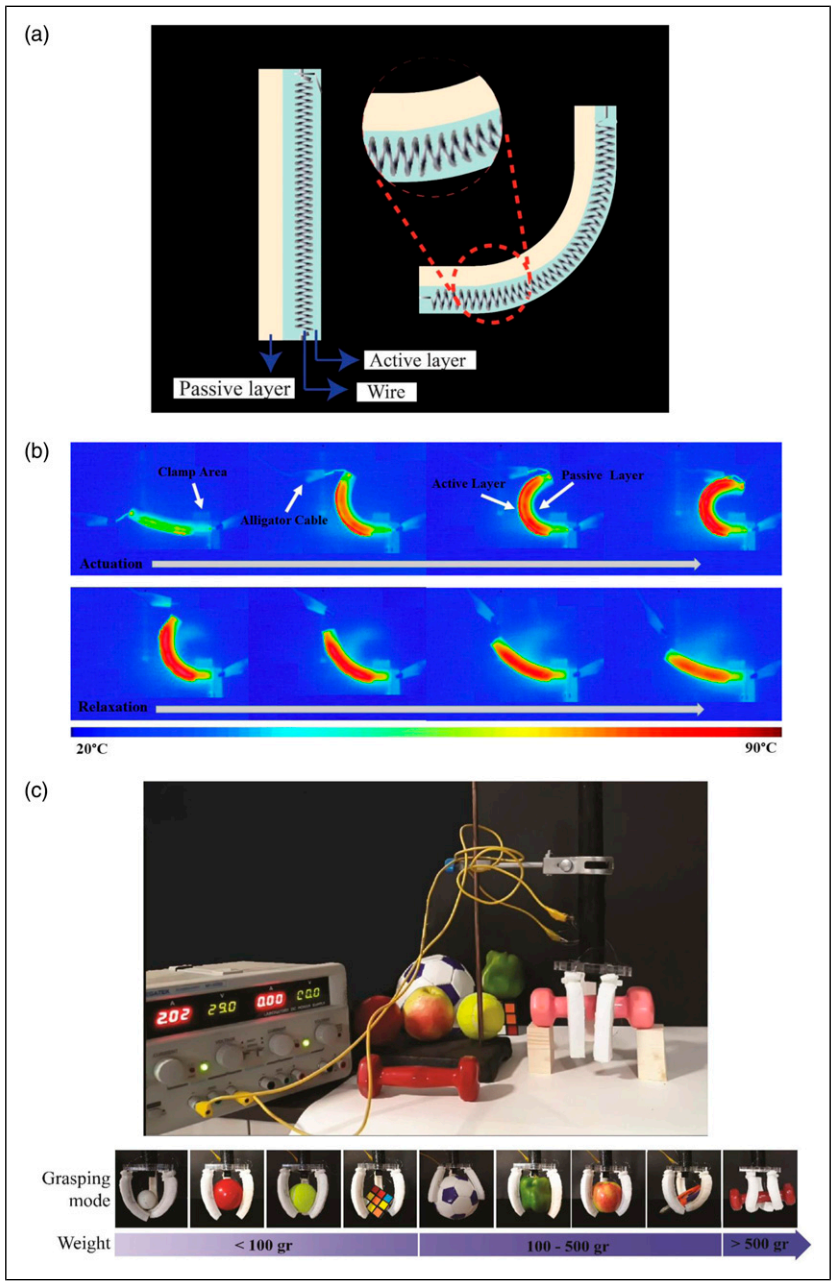

Figure 9. Implementation of the soft composite actuator as a Finger-type gripper. (a) Design of the bending actuator, (b) Schematic of the composite bending operation, (c) Demonstration of grasping and lifting objects with arbitrary shapes and various weights by a soft finger-type gripper.

elongation of the active and passive layers. The constricting force at the vicinity of the passive silicone elastomer layer caused buckling on the passive layer, mimicking natural muscle behavior (Figure 9(a)). Figure 9(b) shows thermal images of a bending actuator operated at 20 W. The high thermal resistance of the passive layer keeps the outer gripping surface at its lowest possible temperature (~40°C) which can be further tuned by increasing the thickness for a safe operation. Figure 9(c) shows three soft bending actuators in finger configuration in series powered at 29 V, 2 A (each finger consumes <20 W). Bending motion occurs upon actuation, and the finger type-soft gripper moves towards the objects and successfully lifts them. The soft finger can carry heavy loads (lift a 500 gr dumbbell) and adapt its shape accordingly to lift objects with arbitrary shapes and weights spanning from less than 10 gr to above 500 gr. We demonstrated the locomotion of the robot in the supplementary movie.

Conclusion

In the present work, we characterized low voltage driven silicone-ethanol soft actuators and presented a paradigm to design a finger-type gripper. To do so, we used the integration of a stimulus-responsive substance (ethanol) in a passive elastomer matrix (silicone). Based on thermal analysis and actuation performance of the samples, 15 wt% was selected as the optimal value of ethanol. The thermogravimetric analysis revealed that the residual ethanol in silicone microcapsules are significantly affected by the weight ratio of ethanol/silicone, in which the most actuation occurs between 50 and 100°C. The evaluation of temperature response revealed that the value of applied power has two main effects on soft composite actuators performance, including 1-the duration of the total working time, 2-the distribution of thermal energy in internal and external composite layers. FE-SEM analysis showed homogeneous distribution of active phase across the entire matrix volume. The material microstructure observation revealed that the diameter-size distribution of inner and outer microcapsules is more narrow and uniform in SE10 than in SE25. Mechanical testing results showed a significant decrease in elastic modulus (1.11 to 0.2 MPa) and tensile strength (3.72 to 1.05 MPa) as a combination of ethanol silicone. The proposed soft actuator demonstrates a high load-to-weight ratio (1000 times greater than its own). We demonstrated the versatility of our electrically driven bending actuator as a soft gripper. The soft finger-type gripper can carry heavy loads and adapt its shape accordingly to lift objects with arbitrary shapes and weights. Finally, we propose two strategies to prevent sample degradation when subjected to temperature changes during a multi-cyclic experiment; one- the development of a protective layer on the actuator surface with low permeability, two- rejuvenation of actuator by immersing it in ethanol, allowing its diffusion into the soft actuator.

Declaration of conflicting interests

The author(s) declared no potential conflicts of interest with respect to the research, authorship, and/or publication of this article.

Funding

The author(s) received no financial support for the research, authorship, and/or publication of this article.

ORCID iD

Samaneh Sahebian https://orcid.org/0000-0001-5378-6615

References

1. Whitesides GM. Soft robotics. *Angew Chem Internat Edit* 2018; 57: 4258–4273.
2. Laschi C, Mazzolai B and Cianchetti M. Soft robotics: technologies and systems pushing the boundaries of robot abilities. *Sci Robot* 2016; 1: eaah3690.
3. Kim S, Laschi C and Trimmer B. Soft robotics: A bioinspired evolution in robotics. *Trends Biotechnol* 2013; 31: 287–294.
4. Rich SI, Wood RJ and Majidi C. Untethered soft robotics. *Nat Electron* 2018; 1: 102–112.
5. Gupta U, Qin L, Wang Y, et al. Soft robots based on dielectric elastomer actuators: a review. *Smart Mater Struct* 2019; 28: 103002.
6. della Santina C, Katzschmann RK, Bicchi A, et al. Editorial: soft robotic modeling and control: bringing together articulated soft robots and soft-bodied robots. *Int J Rob Res* 2021; 40: 3–6.
7. Tian Y, Wang Y, Jin X, et al. Trajectory control and random vibration control of nonlinear system with dielectric elastomer actuator. *Journal of Intelligent Material Systems and Structures* 2018; 29: 2424–2436. DOI: 10.1177/1045389X18770867
8. Trivedi D, Rahn CD, Kier WM, et al. Soft robotics: biological inspiration, state of the art, and future research. *Appl Bionics Biomech* 2008; 5: 99–117.
9. Majidi C. Soft-Matter Engineering for Soft Robotics. *Adv Mater Technol* 2019; 4: 1800477.
10. Kim S, Laschi C and Trimmer B. Soft robotics: a bioinspired evolution in robotics. *Trends Biotechnol* 2013; 31: 287–294.
11. Hughes J, Culha U, Giardina F, et al. Soft manipulators and grippers: a review. *Frontiers Robotics AI* 2016; 3: 69.
12. Runciman M, Darzi A and Mylonas GP. Soft robotics in minimally invasive surgery. *Soft Robot* 2019; 6: 423–443.
13. Rodrigue H, Wei W, Bhandari B, et al. Fabrication of wrist-like SMA-based actuator by double smart soft composite casting. *Smart Mater Struct* 2015; 24: 125003.
14. Hao Y, Wang, Ren, et al. Modeling and experiments of a soft robotic gripper in amphibious environments. *Intern Jour Advan Robotic Sys* 2017; 14, DOI: 10.1177/1729881417707148
15. Rus D and Tolley MT. Design, fabrication and control of soft robots. *Nature* 2015; 521: 467–475.
16. Trivedi D, Rahn CD, Kier WM, et al. Soft robotics: biological inspiration, state of the art, and future research. *Appl Bionics Biomech* 2008; 5: 99–117.
17. Farshad M, Clemens F and Le Roux M. Magnetoactive polymer composite fibers and fabrics -processing and mechanical characterization. *J Thermoplast Compos Mater* 2007; 20: 65–74.
18. Huang WM, Ding, Wang, et al. Shape memory materials. *Mater Today* 2010; 13: 54–61.

19. de Greef A, Lambert P and Delchambre A. Towards flexible medical instruments: Rreview of flexible fluidic actuators. *Precis Eng* 2009; 33: 311–321.
20. Chou CP and Hannaford B. Measurement and modeling of McKibben pneumatic artificial muscles. *IEEE Trans Robot Autom* 1996; 12: 90–102.
21. Tonazzini A, Sadeghi A and Mazzolai B. Electrorheological valves for flexible fluidic actuators. *Soft Robot* 2016; 3: 34–41.
22. Shahinpoor M, Bar-Cohen Y, Simpson JO, et al. Ionic polymer-metal composites (IPMCs) as biomimetic sensors, actuators and artificial muscles - A review. *Smart Mater Struct* 1998; 7.
23. Jain RK, Datta S and Majumder S. Design and control of an IPMC artificial muscle finger for micro gripper using EMG signal. *Mechatronics* 2013; 23: 381–394.
24. Wang X, Khara A and Chen C. A soft pneumatic bistable reinforced actuator bioinspired by Venus Flytrap with enhanced grasping capability. *Bioinspir Biomim* 2020; 15: 056017.
25. Acome E, Mitchell, Morrissey TG, et al. Hydraulically amplified self-healing electrostatic actuators with muscle-like performance. *Science (1979)* 2018; 359, 61–65.
26. Ware T, Ellson, Kwasnik, et al. Tough shape-memory polymer—fiber composites. *J Reinforc Plast Compos* 2011; 30: 371–380.
27. Huang H, Wu L, Lin J, et al. A novel mode controllable hybrid valve pressure control method for soft robotic gripper. *Internat Jour Advan Rob Syste* 2018; 15, DOI: 10.1177/1729881418802140
28. Choudhury M, Mohanty S and Nayak SK Preparation and characterization of carboxyl-treated multiwalled carbon nanotube-reinforced shape-memory polyurethane nanocomposites. *Journ Therm Comp Mat* 2013; 28: 1173–1188. DOI: 10.1177/0892705713503673
29. Robinson RM, Kothera CS and Wereley NM. Variable recruitment testing of pneumatic artificial muscles for robotic manipulators. *IEEE ASME Trans Mechatron* 2015; 20: 1642–1652.
30. Jin B, Song, Jiang, et al. Programming a crystalline shape memory polymer network with thermo- and photo-reversible bonds toward a single-component soft robot. *Sci Adv* 2018; 4.
31. Madsen FB, Daugaard AE, Hvilsted S, et al. The current state of silicone-based dielectric elastomer transducers. *Macromol Rapid Commun* 2016; 37: 378–413.
32. Rinne P, Poldsalu I, Johanson U, et al. Encapsulation of ionic electromechanically active polymer actuators. *Smart Mater Struct* 2019; 28: 074002
33. Kim KJ and Shahinpoor M. A novel method of manufacturing three-dimensional ionic polymer-metal composites (IPMCs) biomimetic sensors, actuators and artificial muscles. *Polymer (Guildf)* 2001; 43: 797–802.
34. Mohd Jani J, Leary M, Subic A, et al. A review of shape memory alloy research, applications and opportunities. *Mater Des* 2014; 56: 1078–1113.
35. Li X, Duan H, Lv P, et al. Soft actuators based on liquid–vapor phase change composites. *Soft Robot* 2021; 8: 251–261.
36. Teeple CB, Koutros TN, Graule MA, et al. Multi-segment soft robotic fingers enable robust precision grasping. *Int J Rob Res* 2020; 39: 1647–1667.
37. Salunkhe PB and Shembekar PS. A review on effect of phase change material encapsulation on the thermal performance of a system. *Renew Sustain Energy Rev* 2012; 16: 5603–5616.
38. Delgado M, Lázaro A, Mazo J, et al. Review on phase change material emulsions and microencapsulated phase change material slurries: Materials, heat transfer studies and applications. *Renew Sustain Energy Rev* 2012; 16: 253–273.

39. Ogden S, Klintberg L, Thornell G, et al. Review on miniaturized paraffin phase change actuators, valves, and pumps. *Microfluid Nanofluidics* 2014; 17: 53–71.
40. Lipton JI, Angle S, Banai RE, et al. Electrically actuated hydraulic solids. *Adv Eng Mater* 2016; 18: 1710–1715.
41. Salaün F, Devaux E, Bourbigot S, et al. Development of phase change materials in clothing part i: formulation of microencapsulated phase change. *Textil Res J* 2010; 80: 195–205.
42. Zhou Z, Li Q, Chen L, et al. A large-deformation phase transition electrothermal actuator based on carbon nanotube-elastomer composites. *J Mater Chem B* 2016; 4: 1228–1234.
43. Chellattoan R, Yudhanto A and Lubineau G. Low-Voltage-driven large-amplitude soft actuators based on phase transition. *Soft Robot* 2020; 7: 688–699.
44. Miriyev A, Stack K and Lipson H. Soft material for soft actuators. *Nat Commun* 2017; 8: 596.
45. Miriyev A, Caires G and Lipson H. Functional properties of silicone/ethanol soft-actuator composites. *Mater Des* 2018; 145: 232–242.
46. Zamyad H and Naghavi N. Behavior identification of IPMC actuators using laguerre-MLP network with consideration of ambient temperature and humidity effects on their performance. *IEEE Trans Instrum Meas* 2018; 67: 2723–2732.
47. Giro-Paloma J, Martínez M, Cabeza LF, et al. Types, methods, techniques, and applications for microencapsulated phase change materials (MPCM): a review. *Renew Sustain Energy Rev* 2016; 53: 1059–1075.
48. Zhang X, Tao X, Yick K, et al. Structure and thermal stability of microencapsulated phase-change materials. *Colloid Polym Sci* 2004; 282: 330–336.
49. Zhang H, Sun S, Wang X, et al. Fabrication of microencapsulated phase change materials based on n-octadecane core and silica shell through interfacial polycondensation. *Colloids Surf A Physicochem Eng Asp* 2011; 389: 104–117.
50. Schiaffino S and Reggiani C. Fiber Types in Mammalian Skeletal Muscles. *Physiol Rev* 2011; 91: 1447–1531. Author Agreement Statement